Acta Astronautica 216 (2024) 37–43

Contents lists available at ScienceDirect

Acta Astronautica

journal homepage: www.elsevier.com/locate/actaastro

Research paper

Mitigating space radiation using magnesium(-lithium) and boron carbide composites

Andrew O'Connor [a], Cheol Park [b], James E. Baciak [a], Michele V. Manuel [a,*]

[a] University of Florida, Gainesville, FL, United States of America
[b] NASA Langley Research Center, Hampton, VA, United States of America

ARTICLE INFO

Keywords:
Galactic cosmic radiation
Secondary neutron
Nuclear fragmentation
Deterministic radiation transport
Low atomic mass metal
Metal matrix composite

ABSTRACT

The health effects of galactic cosmic radiation are a serious impediment to crewed exploration of the solar system. OLTARIS, an interface for the 3DHZETRN deterministic radiation transport code, was used to assess the response of aerospace materials to this constant radiation exposure. Traditional aerospace structural materials like aluminum can, after a certain mass, increase the health effects of such radiation. However, materials with lower atomic mass may mitigate this build-up in secondary radiation with increasing areal density. As such, lower atomic mass structural alloys of magnesium and magnesium–lithium are promising candidates. These alloys may reduce the mass of structures when substituted for aluminum alloys. Reinforcement with boron carbide could further reduce atomic mass while also improving the mechanical properties of such lightweight alloys. This study found that the lower atomic mass of these materials increased nuclear fragmentation upon cosmic radiation interactions, leading to a softening of the secondary (neutron) radiation spectra. This softened spectra reduced the effective dose equivalent, a measure of health effects, for magnesium(-lithium) alloys and their boron carbide-reinforced composites when compared to aluminum.

1. Introduction

Space radiation threatens both human health and microelectronics operation, impacting mission safety [1]. The risks remain difficult to quantify and understand because space radiation energies and types differ so drastically from known terrestrial sources [2]. There are both primary and secondary sources of space radiation. Primary sources include galactic cosmic radiation (GCR), solar particle events (SPEs), and particles trapped by the Earth's magnetosphere [1]. These primary sources also create secondary radiation, primarily neutrons, upon interaction with spacecraft structures due to fragmentation of the structure's nuclei by the incident radiation [1–4]. Understanding how space radiation evolves through its interactions with spacecraft materials, and its eventual effect on equipment and persons, is a continuing challenge in ensuring safe spaceflight [5].

Space radiation risks cannot be eliminated by rote addition of material mass. For instance, several hundred g cm^{-2} of common materials like aluminum (Al) would be necessary to eliminate GCR exposure [6] — an impracticable requirement for mass-constrained spaceflight. Indeed, sufficiently thick materials can actually increase the space radiation risk above from incident radiation alone due to a build-up in radiation (despite an initial decrease) [2–4]. This increase after a certain areal density is due to particle-material reactions and cascades resulting in a "build-up of light particles ($Z < 2$) and localized [secondary radiation] production" near GCR ion tracks [1]. For Al exposed to GCR in free space, the secondary radiation begins to dominate and increases risks above initial beginning around 100 g cm^{-2} to 200 g cm^{-2} [3,4].

As such, the aerospace community continues to investigate advanced, lightweight materials for passive space radiation shielding [7–10]. The 2020 NASA Technology Taxonomy [11] recommends development of lightweight radiation shielding materials (TX06.5.3 "Protection Systems"). It also notes that multifunctional materials also having structural utility can further reduce mass requirements (TX12.1.1 "Lightweight Structural Materials"). Thus, the response of lightweight materials to space radiation is of interest. Al alloys are common in aerospace applications [12–14]. However, magnesium (Mg) alloys have about 35 % lower mass density than Al [15–18]. Recently, Mg alloys have seen renewed interest in the aerospace community due to their lightweight, structural nature [18–21]. Studies have lessened corrosion and flammability concerns [22–25], leading to updates to standards for airplanes and spacecraft have loosened restrictions on the use of Mg alloys [26,27]. Furthermore, alloying Mg with lithium (Li) is especially promising to achieve even further lightweighting [28–30], with some alloys such as Mg-14wt%Li having roughly 24 % lower

* Corresponding author.
E-mail addresses: a.oconnor@ufl.edu (A. O'Connor), cheol.park-1@nasa.gov (C. Park), jebaciak@ufl.edu (J.E. Baciak), mmanuel@ufl.edu (M.V. Manuel).

https://doi.org/10.1016/j.actaastro.2023.12.013
Received 16 June 2023; Received in revised form 5 December 2023; Accepted 8 December 2023
Available online 12 December 2023

mass density than pure Mg. Meanwhile, particle reinforcement, such as boron carbide (B_4C) has been shown to increase the strength and stiffness of these alloys, improving their mechanical properties [31–37]. Furthermore, Mg and Mg-14wt%Li have lower atomic mass than Al, which may mitigate the build-up in space radiation [2,5]. Mg-14wt%Li may also serve as a minor neutron absorber because it should contain some fraction of ^{6}Li that readily absorbs thermal (low energy) neutrons. However, the benefit of such neutron absorption is disputed with respect to space radiation [9]. As such, these lightweight and low atomic mass materials should be investigated for their potential to mitigate space radiation build-up.

Previous studies have shown the evolution of secondary (neutron) radiation with increasing areal density, but these did not include Mg or Mg-14*wt*%Li [3,4,6,9]. This work extends the previous literature by specifically considering Mg and Mg-14*wt*%Li alloys with B_4C addition. The effect of these materials on secondary (neutron) radiation build-up is considered and contrasted with the effect on proton radiation. An updated transport model for the OLTARIS space radiation simulation tool combined with a spherical shell geometry more accurately represents neutron transport. And the use of NASA radiation quality factors aligns this work with the latest NASA space health standard [38]. Ultimately, the ability of Mg and Mg-14*wt*%Li alloys and B_4C addition to mitigate space radiation by suppressing secondary neutron build-up is shown.

2. Material and methods

2.1. Geometry and environmental setup

Pure Al, pure Mg, and Mg-14*wt*%Li in the reinforced and unreinforced conditions were chosen for this study. Reinforcement comprised B_4C added homogeneously to Mg and Mg-14*wt*%Li at 10 % by volume. Areal densities in the range 0.1 g cm^{-2} to 500 g cm^{-2} were explored. The areal densities beyond $50\,\mathrm{g\,cm^{-2}}$ could represent large on-orbit complexes or extraterrestrial habitats [39], especially when considering that a point could see a higher apparent areal density than the thickness of a single wall when the space radiation traverses through multiple nearby walls or other surrounding structures to reach the point under investigation. For example, certain locations on the International Space Station have a higher apparent areal density than the roughly $25\,\mathrm{g\,cm^{-2}}$ of a single wall due to transport through nearby modules and structures [40].

Fig. 1 is a schematic cross-section through the spherical geometries used in this study. The central dot denotes the point detector used for dose tallies and the placement of phantoms. It is surrounded by a 380 cm diameter void region representing the internal spacecraft or module volume. A variable areal density shell composed of the material of interest surrounds this constant void volume. Space radiation is isotropically incident on this shell.

All calculations were performed using the Tool for the Assessment of Radiation in Space (TARIS) version 5.0 using the On-Line TARIS (OLTARIS) interface [41]. TARIS performs 3-dimensional radiation transport using the deterministic High Charge and Energy Transport (3DHZETRN) code. There are still some inaccuracies in 3DHZETRN with respect to its treatment of neutrons with energies less than 20 MeV and electrons [42] despite it performing favorably with Monte Carlo radiation transport codes overall [43]. Results presented here may be more accurate than those generated using prior TARIS versions because photon, electron, positron, muon, and pion transport is now coupled to neutrons and ion transport and transport itself is now 3-dimensional [42]. This 3-dimensional treatment appears necessary to reveal the build-up in dose and protection quantities from GCR seen with increasing areal density [4,6]. The accuracy of neutron transport was further increased by using a spherical (instead of slab) geometry and using a void to represent the interior volume of the spacecraft [40,44]. The radiation tallies were taken at the central point of the sphere instead of throughout the interior volume, which has been argued to improve accuracy [45] although others have questioned its necessity [46]. Overall, the primary purpose of this study is to inform relative structural metal selection so the absolute accuracy of OLTARIS is not as important as the relative trends between the studied materials.

The GCR environment was set to the 1977 solar minimum according to the NASA Design Specification for Natural Environments (DSNE) with boundary conditions computed using the Badhwar-O'Neill 2020 model [44]. All quantities were computed for a period of one Earth year. A free space environment was selected, avoiding the effects of albedo radiation from reflections and interactions with nearby surfaces and structures. GCR at solar minimum provides maximum contribution to the overall space radiation environment [6].

2.2. Response functions

Health risks were evaluated through $H_{Q,T}$ and compared against current NASA limits [38]. Effective dose equivalent was computed using the NASA quality factor ($Q(Z,E)$) relationship [47] and a female phantom[1] (FAX2005 [49]) using "Average US Population" tissue weighting.

OLTARIS does not provide a user-accessible breakdown of dose or $H_{Q,T}$ by particle type. Therefore, dose conversion coefficients (DCCs) from International Commission on Radiological Protection (ICRP) Publication 123 [1] were used to compute whole-body female $H_{Q,T}$ from heavy ions, alphas, protons, neutrons, pion, and muon fluence. Again, $Q(Z,E)$ was used. DCCs from ICRP Publication 116 [50] were used for electrons and photons, assuming isotropic irradiation conditions and sex averaging. Dose conversion coefficients and quality factors were linearly interpolated by energy.

3. Theory

Some results from OLTARIS deserve cautious interpretation. For example, the uncertainties for computations approaching and beyond $500\,\mathrm{g\,cm^{-2}}$ have not been quantified [51]. As OLTARIS only computes between 10^{-2} MeV to 10^6 MeV, radiation exposures outside this energy range, such as thermal neutrons, cannot be assessed. However, the ICRP [1] attributes substantial biological relevance to energies between 10^{-2} MeV to 10^5 MeV for space radiation.[2] Thus, this approach can broadly assess space radiation risks, especially when comparing materials in the same conditions.

After an initial decrease, a sufficiently thick material can paradoxically increase radiation risk in space due to the generation of secondary radiation upon GCR interaction with structures [2–5,52,53]. For instance, primary neutrons are almost non-existent in free-space due to their short lifetimes (approximately 14 min) [54]. Instead, secondary neutrons are generated by incident radiation interactions with the nuclei of surrounding materials and subsequently moderated by further interactions with low-Z nuclei [55]. The magnitude of the build-up is apparently dependent on a material's atomic mass, with low atomic mass materials generating less energetic and massive secondary radiation [2,5,52,56].

Both atomic mass and number of the target nuclei contribute to stopping primary space radiation and to breaking up heavy incident projectiles into less harmful fragments [2,5,52,56]. The Bethe–Bloch relationship for electronic stopping power indicates that increasing atomic number or decreasing atomic mass for the target material (spacecraft structure) will improve the stopping power of a material per unit mass density [5,57], ostensibly reducing exposure from primary

[1] A female phantom was chosen as it typically resulted in higher radiation quantities [48].

[2] Charged particles are evaluated within an even more restrictive range of 1 MeV to 10^5 MeV.

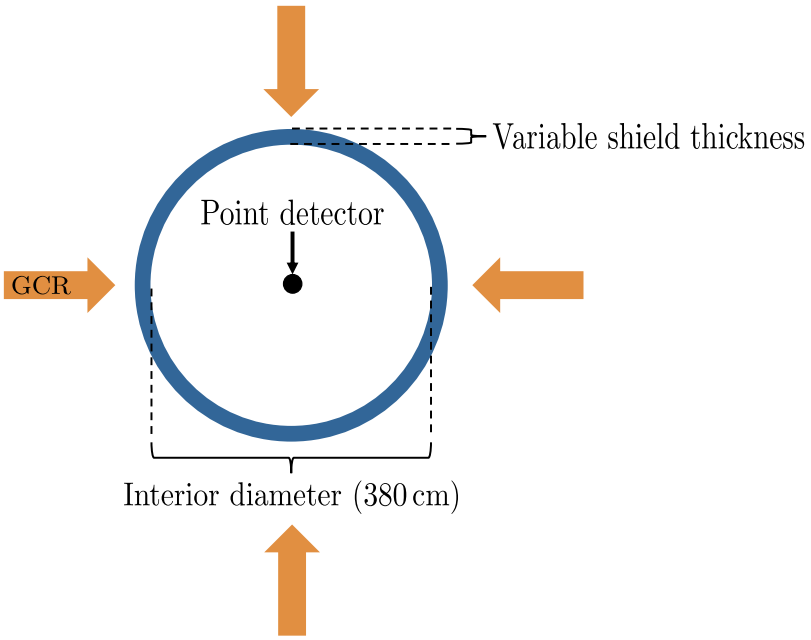

Fig. 1. Notional geometry model for space radiation simulations; cross-section through sphere.

space radiation. Accordingly, low mass yet high charge elements slow down incident ions most effectively on a per mass basis [1,3,52,58].

$$\frac{\sigma}{A_T} \propto A_T^{-1/3} \tag{1}$$

The Bradt–Peters relationship for nuclear fragmentation (Eq. (1)) indicates that decreasing atomic mass of the target (A_T) will increase particle fragmentation (σ) by incident particles per unit mass [5]. Fragmentation breaks up high-Z, high-energy ions (HZE) with high quality factors and linear energy transfer (LET) into less damaging fragments with lower quality factors and LET [2,5], ostensibly reducing protection quantities and thus radiation risks. Therefore, it is typically desirable to use low atomic mass materials[3] [57,58].

4. Results

Table 1 gives both the calculated stopping power and nuclear fragmentation for pure Al, pure Mg, Mg-14*wt*%Li, and B_4C. According to the stopping power metric, Mg and Mg-14*wt*%Li will stop charged particles more effectively than Al with Mg appearing slightly more effective than Mg-14*wt*%Li. However, B_4C is the least effective at stopping charged particles. According to the nuclear fragmentation metric, Mg, Mg-14*wt*%Li, and B_4C are all more liable to cause fragmentation than Al, B_4C being most likely.

4.1. Overall radiation exposure by areal density

In Fig. 2, dose increases with increasing areal density for all materials, becoming especially pronounced after $10\,g\,cm^{-2}$. This is the conventional build-up in radiation exposure with increasing thickness due to secondary radiation generation. Initially, the increase in radiation from this secondary particles outpaces the attenuation of primary GCR. However, after a certain thickness, more secondary radiation is eliminated than produced and thus the overall radiation exposure begins to decrease [4,39,59]. Magnesium and Mg-14*wt*%Li reduce dose compared to Al at areal densities less than $100\,g\,cm^{-2}$ but increase beyond this point. The relative increase at higher areal densities may be due to increased fragmentation, leading to the increased production of secondary radiation. Boron carbide addition increases dose at nearly all thicknesses, becoming apparent beyond $10\,g\,cm^{-2}$. As B_4C has the lowest atomic mass of all studied materials (Table 1), this supports increased dose as being due to increased fragmentation which generates additional secondary radiation.

Table 1
Stopping power (S/ρ) and nuclear fragmentation (σ/A_T) metrics indicating that Mg and Mg-14wt%Li are more effective than Al at stopping charged particles while B_4C is less effective and that Al is the least liable to cause fragmentation.

Material	S/ρ	σ/A_T
Al	0.482	0.333
Mg	0.494	0.345
Mg-14wt%Li	0.491	0.358
B_4C	0.471	0.449

In Fig. 3, effective dose equivalent ($H_{Q,T}$) initially decreases with increasing areal density up to $20\,g\,cm^{-2}$ but then builds-up similarly to dose with a peak around $200\,g\,cm^{-2}$. At its maximum, $H_{Q,T}$ exceeds the 600 mSv NASA career limit[4] on an annual basis. Mg and Mg-14*wt*%Li clearly reduce $H_{Q,T}$ compared to Al beyond $1\,g\,cm^{-2}$ and especially reduce it near $100\,g\,cm^{-2}$ to $300\,g\,cm^{-2}$. This contrasts with the increase in dose seen for Mg and Mg-14*wt*%Li (Fig. 2). Fig. 3 also shows that B_4C addition clearly reduces $H_{Q,T}$ beyond $50\,g\,cm^{-2}$ despite also increasing the dose at these same areal densities (Fig. 2). The maximum extent of reduction in $H_{Q,T}$ through Mg and Mg-14*wt*%Li substitution or B_4C addition is centered about 200 MeV and is roughly 10 % at most.

4.2. Radiation exposure by type and energy

Investigation of radiation exposure at constant areal density allows differentiation between materials by radiation type and energy. An

[3] Paradoxically, lower-energy secondaries may cause a higher dose than the originally incident GCR particle since they are more numerous and may be more penetrating [53,57]. However, these lower-energy secondaries may have lower quality factors and thus reduce protection quantities overall.

[4] The career limit for all astronauts has been set to an $H_{Q,T}$ of 600 mSv, irrespective of age or sex [38].

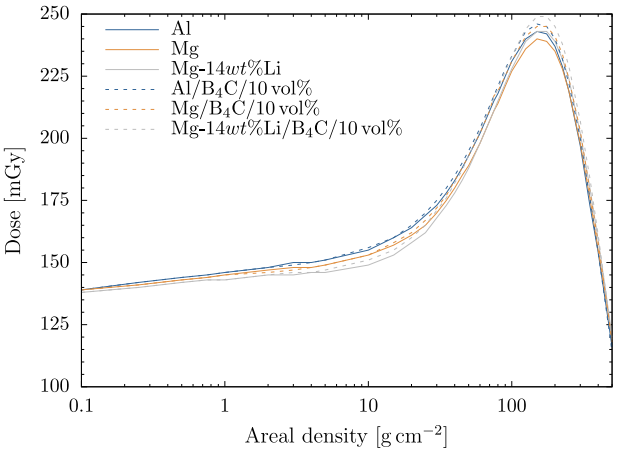

Fig. 2. Mg and Mg-14*wt*%Li initially reduce annual dose before the trend becomes inconsistent; B_4C slightly increases annual dose.

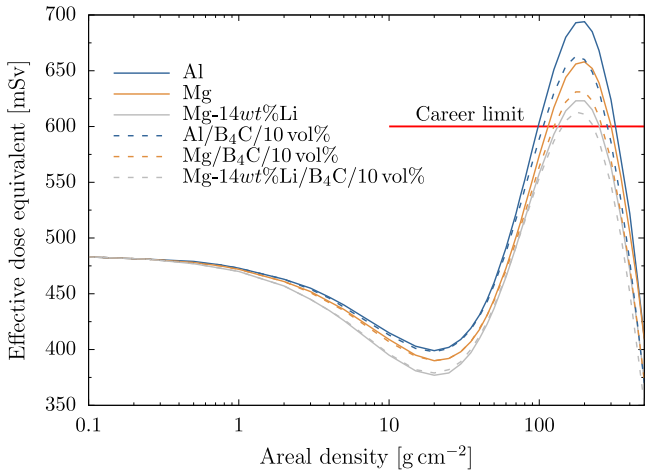

Fig. 3. Mg and Mg-14*wt*%Li reduce annual effective dose equivalent by $1\,g\,cm^{-2}$ while the reduction from B_4C addition appears by $100\,g\,cm^{-2}$.

areal density of $100\,g\,cm^{-2}$ was chosen because it is near the typical crossover point where the build-up of secondary radiation exceeds the reduction in primary radiation and it is where Mg-14*wt*%Li exceeds the NASA career limit. As aforementioned, previous literature indicated that protons and neutrons are the greatest contributors to primary and secondary radiation, respectively, at this point [3,4]. Additional results from OLTARIS for other radiation types such as heavy ions, alpha particles, and muons indicated that these were not substantial contributions to radiation exposure at this areal density. There was some build-up in electrons, photons, and pions, but their contribution to $H_{Q,T}$ was much lower than that of protons and neutrons at this areal density. Fig. 4 demonstrates how increases in secondary radiation – mostly neutrons with some pions, photons, electrons, and secondary protons – outweighed the decrease in primary radiation – mostly heavy ions like ^{16}O, alpha particles, and primary protons – until thicknesses exceeding $100\,g\,cm^{-2}$. As such, protons and neutrons were chosen as the focus of this study.

Fig. 5 gives the fluences by radiation type in the chosen materials. Proton fluence varies little with target material — Mg-14*wt*%Li and B_4C additions slightly increase fluence in the range 100 MeV to 2000 MeV, but the trend for Mg is inconsistent. This slight increase may result from fragmentation leading to the enhanced generation of lower mass projectiles like protons [56]. Conversely, neutron fluence varies substantially with target material. There is a small increase for Mg, Mg-14*wt*%Li, and B_4C addition around 100 MeV and a somewhat larger

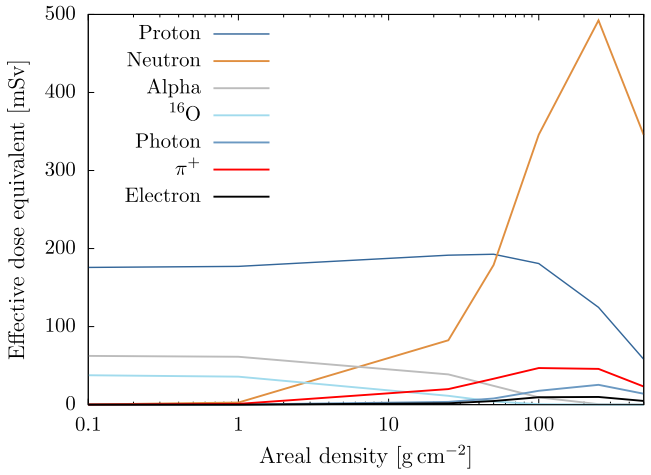

Fig. 4. Protons and neutrons dominate annual $H_{Q,T}$ by areal density in Al.

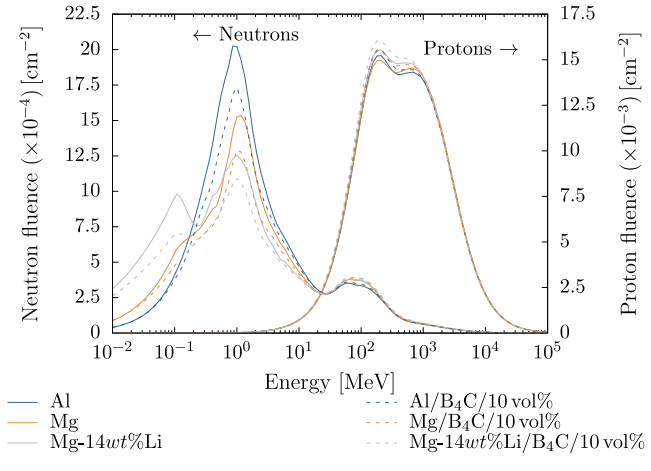

Fig. 5. At $100\,g\,cm^{-2}$, Mg and Mg-14*wt*%Li, and B_4C addition shift annual neutron fluence from more to less energetic regions; there is not much difference by material for annual proton fluence.

increase below around 0.2 MeV. However, there is a strong reduction for Mg, Mg-14*wt*%Li, and B_4C addition between 0.2 MeV to 20 MeV, compared to Al. Mg reduces neutron fluence by approximately 25 % and Mg-14*wt*%Li by nearly 40 % at the maximum extent near 1 MeV. Boron carbide addition further reduces neutron fluence by roughly 20 % for all matrices. There is a noticeable shift from higher to lower neutron energies with respect to integrated fluence. This is probably not due to neutron absorption by ^{10}B in B_4C as the neutrons in this study are too energetic for substantial absorption. As such, this shift from higher to lower neutron energies may be attributed to increased nuclear fragmentation due to lower atomic mass, thereby generating lower energy and quality projectiles [52,56].

Fig. 6 shows that there is a small increase in $H_{Q,T}$ from protons below 1000 MeV for Mg, Mg-14*wt*%Li, and B_4C addition. For $H_{Q,T}$ from neutrons, Mg, Mg-14*wt*%Li, and B_4C addition greatly suppress the build-up between 0.2 MeV to 20 MeV — the same range of fluence depression. The increase in fluence below 0.2 MeV does not result in a substantial increase in $H_{Q,T}$ as the $Q(Z,E)$ is much lower in this range than for that where the fluence is depressed. While there is some increase in $H_{Q,T}$ from neutrons above 30 MeV, this is much smaller in absolute terms than the reduction at lower energies. Thus, the neutron fluence depression occurs precisely in the most biologically impactful energy range, intensifying the overall $H_{Q,T}$ reduction.

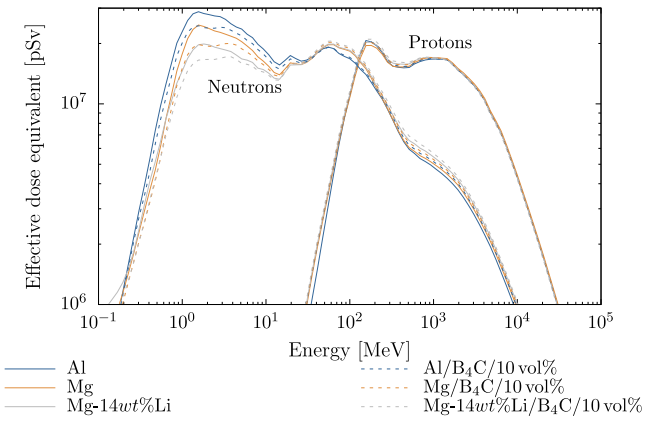

Fig. 6. At 100 g cm^{-2}, Mg and Mg-14*wt*%Li, and B_4C addition reduce annual $H_{Q,T}$ from neutrons in the biologically relevant range from 0.2 MeV to 20 MeV while that from protons is relatively unaffected.

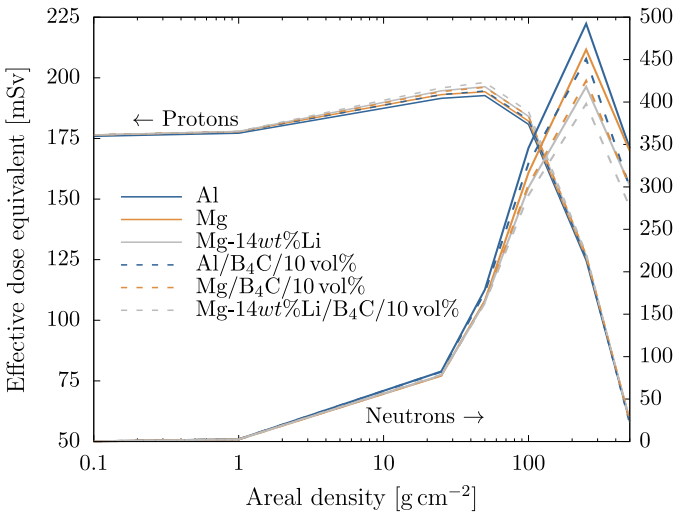

Fig. 7. Mg, Mg-14*wt*%Li, and B_4C addition slightly increase annual $H_{Q,T}$ from protons beyond 1 g cm^{-2} while that from neutrons is reduced beyond 25 g cm^{-2}.

4.3. Proton and neutron radiation exposure by areal density

Integrating $H_{Q,T}$ by radiation type enables analysis of the evolution of the space radiation risk by primary and secondary contributions. Thus, the influence of target material – and its atomic mass – can be readily evaluated.

Fig. 7 shows that $H_{Q,T}$ from protons remains unchanged until 1 g cm^{-2}, then builds up to a maximum around 40 g cm^{-2}, and finally rapidly decreases beyond this. In the build-up region, Mg/Mg-14*wt*%Li and B_4C additions slightly increase $H_{Q,T}$ compared to Al. This may be a result of nuclear fragmentation increasing lower mass projectiles like protons rather than ions [56]. The maximal increase is slight, not exceeding 3.5 % over Al.

Fig. 7 also shows that $H_{Q,T}$ from neutrons shows a consistent and substantial reduction with Mg/Mg-14*wt*%Li and B_4C addition compared to Al. The build-up also demonstrates the solely secondary nature of these neutrons. Beyond about 25 g cm^{-2}, Mg and Mg-14*wt*%Li reduce $H_{Q,T}$ from neutrons by about 20 % at maximum. In this same areal density range, B_4C addition also reduces $H_{Q,T}$ by about 10 % at maximum. This reduction in neutron $H_{Q,T}$ appears responsible for the reduction in overall $H_{Q,T}$ build-up as seen in Fig. 3. While protons constitute a substantial but not majority of overall $H_{Q,T}$ prior to 100 g cm^{-2}, neutrons are mostly responsible for $H_{Q,T}$ past this. Thus, the suppression in neutron build-up suppresses overall $H_{Q,T}$ build-up. The consistent reduction in $H_{Q,T}$ from neutrons may be attributed to the decrease in energetic neutrons with a high $Q(Z,E)$ and the increase in neutrons being less energetic ones with a comparatively low $Q(Z,E)$ as shown in Figs. 5 and 6. Increased fragmentation by lower atomic mass materials leads to lower mass projectiles like protons and neutrons [52,56] and, importantly, generates these projectiles in less biologically relevant energies — at least for neutrons weighted according to $Q(Z,E)$.

5. Discussion

Dose, depicted in Fig. 2, shows the conventional build-up with increasing areal density due to secondary radiation generation from nuclear fragmentation of the target material's nuclei. Pure Mg and Mg-14*wt*%Li reduce dose before 100 g cm^{-2} despite having an inconsistent trend beyond this. Interestingly, B_4C addition causes a relative increase in dose at most areal densities. The effective dose equivalent ($H_{Q,T}$) exhibits a two-stage suppression profile with Mg, Mg-14*wt*%Li, and B_4C addition: a moderate 5 % reduction at lower areal densities and a larger 10 % to 15 % reduction at great areal densities.

Fig. 7 indicates that pure Mg, Mg-14*wt*%Li, and B_4C addition reduce $H_{Q,T}$ compared to Al mostly due to the reduction in neutron build-up. This may be due to increased fragmentation of the lower atomic mass nuclei in these materials, leading to lower mass and less energetic and less deleterious projectiles. These trends from lower atomic mass materials comport with the relative increase in nuclear fragmentation relative to Al predicted from Table 1. Mg, Mg-14*wt*%Li, and B_4C addition increase the proton dose and $H_{Q,T}$ relative to Al. However, this increase is small in absolute terms. The increase in charged radiation may be attributed to a shift in lighter fragmentation products from lighter nuclei in the lightweight materials [52,56]. Bond et al. [9] found a similar benefit to lighter elements and materials, though they did not describe the composition of the secondary radiation produced.

The majority of build-up beyond 100 g cm^{-2} arises from secondary neutrons and not protons (Fig. 7). This is in contradistinction to the findings of Slaba et al. [4] who claimed that protons were the largest contributor to build-up. This discrepancy may be resolved by noting that the referenced study only evaluated areal densities up to 100 g cm^{-2}, did not use a spherical geometry, and reported dose equivalent using the ICRP Publication 60 quality factor ($Q(L)$). There is a benefit to Mg/Mg-14*wt*%Li and B_4C composites with respect to dose and, especially, $H_{Q,T}$ build-up in most circumstances evaluated. This benefit is apparently due to suppression of the secondary neutron contribution, which dominates the overall $H_{Q,T}$ at high areal densities. This suppression arises from the spectral softening of the neutron contribution from energetic and high $Q(Z,E)$ to less energetic and lower $Q(Z,E)$. Mg, Mg-14*wt*%Li, and B_4C addition leads to this spectral softening. The decrease in mass of projectiles from fragmentation apparently also extends to a softening in their energy spectra, reducing their $Q(Z,E)$ and thus health risks as shown by $H_{Q,T}$. Horst et al. [39] similarly ascribed the build-up in radiation as due to secondary neutrons, but instead suggested a two-layer polyethylene shielding to attenuate neutron produced in an initial Al layer rather than the present study's findings of secondary neutron suppression from inherently lower atomic mass metals and composites.

6. Conclusions

Pure Mg and Mg-14*wt*%Li can substitute for Al, resulting in more lightweight aerospace structures. Reinforcement with B_4C may also ameliorate mechanical properties, enabling further lightweighting if component masses can be reduced. Fortuitously, these materials may decrease health risks from space radiation as shown by the reduction in effective dose equivalent compared to Al, especially beyond 10 g cm^{-2}. The reduction relative to Al for lighter materials was found to be at most 5 % for areal densities between 1 g cm^{-2} to 50 g cm^{-2} and a

more substantial 10 % to 15 % reduction at areal densities greater than 50 g cm^{-2}. This reduction is mostly due to a suppression in build-up of secondary neutron radiation, which originates from the lower atomic mass of these materials that increases fragmentation of incident GCR. The secondary neutron contribution to effective dose equivalent is greater than that of primary and secondary protons, the next most substantial contributor, by 50 g cm^{-2} and only increases in relevance beyond this. The build-up in neutrons is shifted from energetic, biologically relevant ranges to less energetic, less biologically relevant ones. The effective dose equivalent builds up less overall and thus space radiation health risks are reduced. Mg and Mg-14*wt*%Li are thus beneficial not only for lightweighting but also space radiation mitigation compared to Al. Boron carbide addition to these metals can additionally mitigate the build-up in secondary space radiation.

Further refinements to the 3DHZETRN code include improved neutron diffusion models and the introduction of data libraries for neutron scattering [60]. This study should be repeated once these changes have been introduced into OLTARIS. Other space radiation environments like SPEs and even artificial radiation sources like nuclear reactors could also be considered.

Declaration of competing interest

The authors declare the following financial interests/personal relationships which may be considered as potential competing interests: This work was supported by a NASA Space Technology Research Fellowship (award 80NSSC19K1163).

Acknowledgments

This work was supported by a NASA Space Technology Research Fellowship, United States of America (award 80NSSC19K1163). Any opinions, findings, and conclusions or recommendations expressed in this material are those of the author(s) and do not necessarily reflect the views of the National Aeronautics and Space Administration. Thanks to Drs Sang-Hyon Chu & Chris Sandridge and Ms Calista Lum for their thoughtful discussions and assistance.

References

[1] ICRP, ICRP publication 123: Assessment of radiation exposure of astronauts in space, Ann. ICRP 42 (2013) http://dx.doi.org/10.1016/j.icrp.2013.05.004.

[2] M. Durante, F.A. Cucinotta, Physical basis of radiation protection in space travel, Rev. Modern Phys. 83 (2011) 1245–1281, http://dx.doi.org/10.1103/RevModPhys.83.1245.

[3] F. Horst, D. Boscolo, M. Durante, F. Luoni, C. Schuy, U. Weber, Thick shielding against galactic cosmic radiation: A Monte Carlo study with focus on the role of secondary neutrons, Life Sci. Space Res. 33 (2022) 58–68, http://dx.doi.org/10.1016/j.lssr.2022.03.003.

[4] T.C. Slaba, A.A. Bahadori, B.D. Reddell, R.C. Singleterry, M.S. Clowdsley, S.R. Blattnig, R.C. Singleterry Jr., M.S. Clowdsley, S.R. Blattnig, Optimal shielding thickness for galactic cosmic ray environments, Life Sci. Space Res. 12 (2017) 1–15, http://dx.doi.org/10.1016/j.lssr.2016.12.003.

[5] M. Durante, Space radiation protection: Destination Mars, Life Sci. Space Res. 1 (2014) 2–9, http://dx.doi.org/10.1016/j.lssr.2014.01.002.

[6] T.C. Slaba, C.J. Mertens, S.R. Blattnig, Radiation Shielding Optimization on Mars, Technical Publication NASA/TP–2013-217983, NASA Langley Research Center, Hampton, VA, 2013.

[7] S.A. Thibeault, J.H. Kang, G. Sauti, C. Park, C.C. Fay, G.C. King, Nanomaterials for radiation shielding, MRS Bull. 40 (2015) 836–841, http://dx.doi.org/10.1557/mrs.2015.225.

[8] M. Naito, S. Kodaira, R. Ogawara, K. Tobita, Y. Someya, T. Kusumoto, H. Kusano, H. Kitamura, M. Koike, Y. Uchihori, M. Yamanaka, R. Mikoshiba, T. Endo, N. Kiyono, Y. Hagiwara, H. Kodama, S. Matsuo, Y. Takami, T. Sato, S. ichi Orimo, Investigation of shielding material properties for effective space radiation protection, Life Sci. Space Res. 26 (2020) 69–76, http://dx.doi.org/10.1016/j.lssr.2020.05.001.

[9] D.K. Bond, B. Goddard, R.C. Singleterry, S. Bilbao y León, Evaluating the effectiveness of common aerospace materials at lowering the whole body effective dose equivalent in deep space, Acta Astronaut. 165 (2019) 68–95, http://dx.doi.org/10.1016/j.actaastro.2019.07.022.

[10] B. Manning, R. Singleterry, Radiation engineering analysis of shielding materials to assess their ability to protect astronauts in deep space from energetic particle radiation, Acta Astronaut. 171 (2020) 23–30, http://dx.doi.org/10.1016/j.actaastro.2020.02.020.

[11] National Aeronautics and Space Administration, 2020 NASA Technology Taxonomy, Technical Report, NASA/HQ, Washington, DC, 2020.

[12] A. Heinz, A. Haszler, C. Keidel, S. Moldenhauer, R. Benedictus, W.S. Miller, Recent development in aluminium alloys for aerospace applications, Mater. Sci. Eng. A 280 (2000) 102–107, http://dx.doi.org/10.1016/S0921-5093(99)00674-7.

[13] T. Ersmark, P. Carlson, E. Daly, C. Fuglesang, I. Gudowska, B. Lund-Jensen, P. Nieminen, M. Pearce, G. Santin, Influence of geometry model approximations on Geant4 simulation results of the Columbus/ISS radiation environment, Radiat. Meas. 42 (2007) 1342–1350, http://dx.doi.org/10.1016/j.radmeas.2007.06.001.

[14] L. Zhu, N. Li, P.R.N. Childs, Light-weighting in aerospace component and system design, Propuls. Power Res. 7 (2018) 103–119, http://dx.doi.org/10.1016/j.jppr.2018.04.001.

[15] M.K. Kulekci, Magnesium and its alloys applications in automotive industry, Int. J. Adv. Manuf. Technol. 39 (2008) 851–865, http://dx.doi.org/10.1007/s00170-007-1279-2.

[16] T.M. Pollock, Weight loss with magnesium alloys, Science 328 (2010) 986–987, http://dx.doi.org/10.1126/science.1182848.

[17] J. Song, J. Chen, X. Xiong, X. Peng, D. Chen, F. Pan, Research advances of magnesium and magnesium alloys worldwide in 2021, J. Magnes. Alloys 10 (2022) 863–898, http://dx.doi.org/10.1016/j.jma.2022.04.001.

[18] A. Wendt, K. Weiss, A. Ben-Dov, M. Bamberger, B. Bronfin, Magnesium castings in aeronautics applications - Special requirements, in: N.R. Neelameggham, H.I. Kaplan (Eds.), Magnesium Technology, No. 2005, 2005, pp. 65–69.

[19] I. Ostrovsky, Y. Henn, Present state and future of magnesium application in aerospace industry, in: International Conference New Challenges in Aeronautics, ASTEC'07, Moscow, Russia, 2007.

[20] S.R. Agnew, N.R. Neelameggham, E.A. Nyberg, A. Wendt, S.N. Mathaudhu, E.A. Nyberg, Magnesium Alloys in U.S. military applications: Past, current and future solutions, in: Magnesium Technology, No. 2010, 2010, pp. 71–76.

[21] T. Homma, N. Kunito, S. Kamado, Fabrication of extraordinary high-strength magnesium alloy by hot extrusion, Scr. Mater. 61 (2009) 644–647, http://dx.doi.org/10.1016/j.scriptamat.2009.06.003.

[22] M. Dhawan, C. Wright, T. Johnson, D. Parker, P. Howard, M. Manuel, D. Christianson, P. Spencer, S. Harper, F. Juarez, J. Aroh, P. Lyon, Development and flammability testing of magnesium alloys for space applications, 2018, URL: https://ntrs.nasa.gov/citations/20180004949.

[23] M.C. Wright, E.L. Montgomery, M.V. Manuel, IRTD Proposal FY17: Flammability and corrosion testing of lightweight magnesium alloys for mass reduction and radiation mitigation in spacecraft applications, 2019, URL: https://ntrs.nasa.gov/citations/20190032990.

[24] P. Predko, D. Rajnovic, M.L. Grilli, B.O. Postolnyi, V. Zemcenkovs, G. Rijkuris, E. Pole, M. Lisnanskis, Promising methods for corrosion protection of magnesium alloys in the case of Mg-Al, Mg-Mn-Ce and Mg-Zn-Zr: A recent progress review, Metals 11 (2021) 1133, http://dx.doi.org/10.3390/met11071133.

[25] T.R. Marker, Evaluating the Flammability of Various Magnesium Alloys During Laboratory- and Full-Scale Aircraft Fire Tests, Final Report DOT/FAA?AR-11/3, Federal Aviation Administration, Atlantic City, NJ, 2014, URL: https://www.fire.tc.faa.gov/pdf/AR11-13.pdf.

[26] Standard materials and processes requirements for spacecraft, 2021, URL: https://standards.nasa.gov/sites/default/files/standards/NASA/C//2021-09-30-NASA-STD-6016C-Approved.pdf.

[27] Performance standard for seats in civil rotorcraft, transport aircraft, and general aviation aircraft, 2015, URL: https://www.sae.org/standards/content/as8049c/.

[28] F. Schott, D. McKeown, L. Jin, M. Celikin, Development of magnesium–lithium-based alloys for space applications: The relationship between precipitation hardening and damping capacity, in: P. Maier, S. Barela, V.M. Miller, N.R. Neelameggham (Eds.), Magnesium Technology 2022, Springer International Publishing, Cham, 2022, pp. 77–81.

[29] H. Haferkamp, R. Boehm, U. Holzkamp, C. Jaschik, V. Kaese, M. Niemeyer, Alloy development processing and applications in magnesium lithium alloys, Mater. Trans. 42 (2001) 1160–1166, http://dx.doi.org/10.2320/matertrans.42.1160.

[30] P.D. Frost, Technical and Economic Status of Magnesium-Lithium Alloys, Special Publication NASA/SP-5028, National Aeronautics and Space Administration, Washington, DC, 1965.

[31] D. Lee, J. Kim, B. Park, I. Jo, S.-K. Lee, Y. Kim, S.-B. Lee, S. Cho, Mechanical and thermal neutron absorbing properties of B4C/Aluminum alloy composites fabricated by stir casting and hot rolling process, Metals 11 (2021) 413, http://dx.doi.org/10.3390/met11030413.

[32] H. Guo, Z. Zhang, Y. Zhang, Y. Cui, L. Sun, D. Chen, Improving the mechanical properties of B4C/Al composites by solid-state interfacial reaction, J. Alloys Compd. 829 (2020) 154521, http://dx.doi.org/10.1016/j.jallcom.2020.154521.

[33] E. Ghasali, M. Alizadeh, M. Niazmand, T. Ebadzadeh, Fabrication of magnesium-boron carbide metal matrix composite by powder metallurgy route: Comparison between microwave and spark plasma sintering, J. Alloys Compd. 697 (2017) 200–207, http://dx.doi.org/10.1016/j.jallcom.2016.12.146.

[34] H.-S. Chen, W.-X. Wang, Y.L. Li, P. Zhang, H.H. Nie, Q.C. Wu, The design, microstructure and tensile properties of B4C particulate reinforced 6061Al neutron absorber composites, J. Alloys Compd. 632 (2015) 23–29, http://dx.doi.org/10.1016/J.JALLCOM.2015.01.048.

[35] L. Chen, Y. Yao, Processing, microstructures, and mechanical properties of magnesium matrix composites: A review, Acta Metall. Sin. (Engl. Lett.) 27 (2014) 762–774, http://dx.doi.org/10.1007/s40195-014-0161-0.

[36] Y. Li, W.-X. Wang, J. Zhou, H.-S. Chen, P. Zhang, 10B areal density: A novel approach for design and fabrication of B4C/6061Al neutron absorbing materials, J. Nucl. Mater. 487 (2017) 238–246, http://dx.doi.org/10.1016/J.JNUCMAT.2017.02.020.

[37] Y. h. Sun, R. c. Wang, C. q. Peng, Y. Feng, M. Yang, Recent progress in Mg-Li matrix composites, Trans. Nonferr. Met. Soc. China 29 (2019) 1–14, http://dx.doi.org/10.1016/S1003-6326(18)64909-X.

[38] National Aeronautics and Space Administration, NASA Space Flight Human-System Standard: Volume 1: Crew Health, NASA TECHNICAL STANDARD 3001, Vol. 1, Rev. B, NASA Headquarters, Washington, DC, 2022.

[39] F. Horst, D. Boscolo, G. Cartechini, M. Durante, C. Hartel, E. Kozlova, C. La Tessa, M. Missiaggia, E. Pierobon, T. Radon, R. Ridolfi, S. Ritter, C. Schuy, A. Sokolov, U. Weber, M. Zbořil, A multi-detector experimental setup for the study of space radiation shielding materials: Measurement of secondary radiation behind thick shielding and assessment of its radiobiological effect, in: EPJ Web of Conferences, in: EDP Sciences, vol. 261, Prague, Czechia, 2022, p. 03002, http://dx.doi.org/10.1051/epjconf/202226103002.

[40] J. Barthel, N. Sarigul-Klijn, Importance of spherical shell models for radiation shielding designs on space missions, J. Spacecr. Rockets 56 (2019) 1658–1661, http://dx.doi.org/10.2514/1.A34410.

[41] R.C. Singleterry Jr., S.R. Blattnig, M.S. Clowdsley, G.D. Qualls, C.A. Sandridge, L.C. Simonsen, J.W. Norbury, T.C. Slaba, S.A. Walker, F.F. Badavi, J.L. Spangler, A.R. Aumann, E.N. Zapp, R.D. Rutledge, K.T. Lee, R.B. Norman, OLTARIS: on-Line Tool for the Assessment of Radiation in Space, Technical Publication NASA/TP–2010-216722, NASA Langley Research Center, Hampton, VA, 2010.

[42] T.C. Slaba, J.W. Wilson, C.M. Werneth, K. Whitman, Updated deterministic radiation transport for future deep space missions, Life Sci. Space Res. 27 (2020) 6–18, http://dx.doi.org/10.1016/j.lssr.2020.06.004.

[43] J.W. Wilson, T.C. Slaba, F.F. Badavi, B.D. Reddell, A.A. Bahadori, 3DHZETRN: Neutron leakage in finite objects, Life Sci. Space Res. 7 (2015) 27–38, http://dx.doi.org/10.1016/j.lssr.2015.09.003.

[44] T.C. Slaba, R.C. Singleterry, Correct modeling results are needed to inform mission planning and shield design, Life Sci. Space Res. 25 (2020) 143–147, http://dx.doi.org/10.1016/j.lssr.2019.11.001.

[45] T.C. Slaba, K. Whitman, The Badhwar-O'Neill 2020 GCR Model, Space Weather 18 (2020) http://dx.doi.org/10.1029/2020SW002456.

[46] S. El-Jaby, B.J. Lewis, L. Tomi, A commentary on the impact of modelling results to inform mission planning and shield design, Life Sci. Space Res. 25 (2020) 148–150, http://dx.doi.org/10.1016/j.lssr.2019.11.002.

[47] F.A. Cucinotta, M.-H.Y. Kim, L.J. Chappell, Space Radiation Cancer Risk Projections and Uncertainties – 2012, Technical Publication NASA/TP-2013-217375, NASA Johnson Space Center, Houston, TX, 2013.

[48] T.C. Slaba, G.D. Qualls, M.S. Clowdsley, S.R. Blattnig, S.A. Walker, L.C. Simonsen, Utilization of CAM, CAF, MAX, and FAX for space radiation analyses using HZETRN, Adv. Space Res. 45 (2010) 866–883, http://dx.doi.org/10.1016/j.asr.2009.08.017.

[49] R. Kramer, H.J. Khoury, J.W. Vieira, E.C.M. Loureiro, V.J.M. Lima, F.R.A. Lima, G. Hoff, All about FAX: A Female Adult voXel phantom for Monte Carlo calculation in radiation protection dosimetry, Phys. Med. Biol. 49 (2004) 5203, http://dx.doi.org/10.1088/0031-9155/49/23/001.

[50] N. Petoussi-Henss, W. Bolch, K. Eckerman, A. Endo, N. Hertel, J. Hunt, M. Pelliccioni, H. Schlattl, M. Zankl, ICRP Publication 116: Conversion coefficients for radiological protection quantities for external radiation exposures, Ann. ICRP 40 (2010) 1–257, http://dx.doi.org/10.1016/j.icrp.2011.10.001.

[51] C.A. Sandridge, Personal communication, 2022.

[52] J.W. Wilson, J. Miller, A. Konradi, F.A. Cucinotta (Eds.), Shielding Strategies for human space exploration, in: ASA Conference Publication 3360, NASA Langley Research Center, Houston, TX, 1997, pp. iii–481.

[53] K.A. More, O.L. Tiffany, Cosmic-Ray Shower Production in Manned Space Vehicles - Copper, NASA/SP-71, NASA, Gatlinburg, TN, 1964, pp. 183–188, URL: https://ntrs.nasa.gov/citations/19650024998.

[54] J.W. Norbury, W. Schimmerling, T.C. Slaba, E.I. Azzam, F.F. Badavi, G. Baiocco, E. Benton, V. Bindi, E.A. Blakely, S.R. Blattnig, D.A. Boothman, T.B. Borak, R.A. Britten, S. Curtis, M. Dingfelder, M. Durante, W.S. Dynan, A.J. Eisch, S.R. Elgart, D.T. Goodhead, P.M. Guida, L.H. Heilbronn, C.E. Hellweg, J.L. Huff, A. Kronenberg, C. La Tessa, D.I. Lowenstein, J. Miller, T. Morita, L. Narici, G.A. Nelson, R.B. Norman, A. Ottolenghi, Z.S. Patel, G. Reitz, A. Rusek, A.-S. Schreurs, L.A. Scott-Carnell, E. Semones, J.W. Shay, V.A. Shurshakov, L. Sihver, L.C. Simonsen, M.D. Story, M.S. Turker, Y. Uchihori, J. Williams, C.J. Zeitlin, Galactic cosmic ray simulation at the NASA Space Radiation Laboratory, Life Sci. Space Res. 8 (2016) 38–51, http://dx.doi.org/10.1016/j.lssr.2016.02.001.

[55] L.H. Heilbronn, T.B. Borak, L.W. Townsend, P.-E. Tsai, C.A. Burnham, R.A. McBeth, Neutron yields and effective doses produced by Galactic Cosmic Ray interactions in shielded environments in space, Life Sci. Space Res. 7 (2015) 90–99, http://dx.doi.org/10.1016/J.LSSR.2015.10.005.

[56] J.H. Adams, D.H. Hathaway, R.N. Grugel, J.W. Watts, T.A. Parnell, J.C. Gregory, R.M. Winglee, Revolutionary Concepts of Radiation Shielding for Human Exploration of Space, Technical Memorandum NASA/TM-2005-213688, NASA/MSFC, Huntsville, AL, 2005, URL: http://hdl.handle.net/2060/20050180620.

[57] C. Zeitlin, D.M. Hassler, R.F. Wimmer-Schweingruber, B. Ehresmann, J. Appel, T. Berger, E. Böhm, S. Böttcher, D.E. Brinza, S. Burmeister, J. Guo, J. Köhler, H. Lohf, C. Martin, D. Matthiä, A. Posner, S. Rafkin, G. Reitz, Y.D. Tyler, M. Vincent, G. Weigle, Y. Iwata, H. Kitamura, T. Murakami, Calibration and characterization of the radiation assessment detector (RAD) on curiosity, Space Sci. Rev. 201 (2016) 201–233, http://dx.doi.org/10.1007/s11214-016-0303-y.

[58] J.W. Wilson, F.M. Denn, Preliminary Analysis of the Implications of Natural Radiations on Geostationary Operations, Technical Note NASA/TN-D-8290, NASA Langley Research Center, Hampton, VA, 1976, URL: https://ntrs.nasa.gov/citations/19760026032.

[59] G. Pfotzer, Dreifachkoinzidenzen der Ultrastrahlung aus vertikaler Richtung in der StratosphÄre, Z. Phys. 102 (1936) 23–40, http://dx.doi.org/10.1007/BF01336829.

[60] J.W. Wilson, T.C. Slaba, C.M. Werneth, F.F. Badavi, B.D. Reddell, A.A. Bahadori, Neutron Diffusion Correction in 3DHZETRN-, Technical Publication NASA/TP-20210020403, NASA/LaRC, Hampton, VA, 2021.